Impact of multi-component description of hydrophilic fuel droplets in propagating spray flames

Fernando Luiz Sacomano Filho, Luís Eduardo de Albuquerque Paixão E Freire de Carvalho, Artur Carvalho Santos, Aymeric Vié, Jeroen Adrianus van Oijen

Impact of multi-component description of hydrophilic fuel droplets in propagating spray flames

Fernando Luiz Sacomano Filho[a,*], Luís Eduardo de Albuquerque Paixão e Freire de Carvalho[a], Artur Carvalho Santos[b], Aymeric Vié[b,c], Jeroen Adrianus van Oijen[d]

[a]*Laboratory of Environmental and Thermal Engineering, Universidade de São Paulo, São Paulo, Brazil.*
[b]*Laboratoire EM2C, CNRS, CentraleSupelec, Université Paris-Saclay, Gif-sur-Yvette, France.*
[c]*Fédération de Mathématiques, CentraleSupelec, Université Paris-Saclay, Gif-sur-Yvette, France.*
[d]*Department of Mechanical Engineering, Technische Universiteit Eindhoven, Eindhoven, The Netherlands.*

Abstract

The need for an accurate description of the liquid composition is emerging in recently published studies on the interaction of droplets and flames. The selective release of species from a droplet surface into a reacting flow has been shown to impact the evolution of chemical reactions. However, preference has been given to hydrocarbons. Hydrophilic fuels were not explored enough to allow a broad perception of the importance of considering the multi-component description of liquid droplets in reacting flows. This may be justified by the limitations of the modeling strategies, which could not describe the simultaneous occurrence of evaporation and condensation for different species. Such limitations have been recently overcome by a new phase change model [1]. Given these aspects, this work investigates the impact of accurately describing the heat and mass transfers on droplets interacting with flames. Numerical simulations of freely propagating flames in droplet mists are conducted with a detailed chemistry description. Different scenarios focus on the impact of water addition in the gaseous or in the liquid phase. Results demonstrated that accounting for the multi-component phase change significantly impacts the flame speed. This is shown to be a consequence of the hydrophilic property of the chosen fuel, which allows the conversion from single-component to multi-component droplets, thus modifying the flame structure.

Keywords: Multi-component droplets, Spray combustion, Phase change modeling, Differential diffusion, Ethanol

Novelty and significance statement

- Differential diffusion is rigorously accounted for with a new phase change model in flames propagating in droplet mists of a hydrophilic fuel, i.e. ethanol.
- The multi-component modeling is demonstrated to be necessary even when considering the injection of a pure hydrophilic fuel.

*Corresponding author
Email address: fernando.sacomano@usp.br (Fernando Luiz Sacomano Filho)

- When the multi-component description of the liquid fuel is enabled, flame speeds become higher than those values achieved with the single-component approach.
- Air humidity interacts with hydrophilic fuel droplets delivering higher flame speed values.
- A novel justification is presented for the observed higher flame speed values of flames propagating in droplets mists when compared to single phase flames.

Author contributions statement

F.L.S.F.: designed and performed research, analyzed and post-processed data, and wrote the paper. L.E.A.P.F.C.: performed simulations, analyzed and post-processed data, revised the paper. A.C.S.: supported the model implementations, analyzed data, revised the paper. A.V.: provided algorithms, analyzed data, revised the paper. J.A.v.O.: provided software, analyzed data, revised the paper.

1. Introduction

Typical commercial fuels are composed of a large number of species, and require multi-component modeling for the numerical description of spray flames [1–4]. Investigations about the multi-component description of droplets in non-reacting atmospheres are found in the literature for single droplets (e.g. [1, 4–11]) and spray flows (e.g. [12]). However, the interaction of multi-component droplets with reacting flows is not extensively explored. Spray combustion simulations are commonly conducted with single-component surrogate fuels (e.g. [13, 14]) to avoid the complexity of modeling chemical reactions and droplet phase change.

From the published works accounting for multi-component droplets in reacting flows (e.g. [2, 3, 15–21]), both [2, 3] stand out. Shastry et al. [2] investigated one-dimensional flames propagating in multi-component sprays using a detailed description of the chemistry. Alkane mixtures representing Jet-A surrogates are evaluated following the ideal vapor-liquid equilibrium (VLE) approach and without considering differential diffusion of vapor into the gas flow. The importance of the multi-component description of droplets is noticed in terms of the stratified mass exchange caused by the different vapor pressures of different components. Differential diffusion effects in reacting flows are included in [3], which also investigates alkane mixtures representing Jet-A surrogates. 1D Counterflow spray flames were simulated using a detailed description of the chemistry. Results outline that differential diffusion effects are necessary for modeling multi-component spray combustion.

All these previous studies considered mixtures of long hydrocarbons. When considering alcohols, the number of species is usually small in a commercial fuel (e.g. ethanol). However, these hydrophilic substances can absorb the air humidity and the water formed during combustion [1, 22, 23]. This aspect reinforces the importance of the multi-component description of droplets for both reacting and non-reacting atmospheres. Another important aspect is the limitations of different models available in the literature to accurately describe droplets' heat and mass transfer process in reacting atmospheres. Recently, new models were proposed [1, 4], which can accurately describe the differential diffusion of vapor into the carrier phase for hydrophilic and non-hydrophilic droplets interacting with general reacting flows.

Within the context of one-dimensional simulations conducted with a detailed description of the chemistry, flames propagating in droplet mists have been demonstrated as an important setup to fulfill an old gap in the research of spray combustion. As well observed by Versaevel [24], spray combustion test cases are mainly found in two extreme setups: single-droplet or polydisperse disperse flows. The last case predominantly involves turbulent carrier phase flows and is not far from real application flames, which implies complex flow configurations. Since that study, new experimental and numerical setups have been proposed (e.g. [6, 25–28]) to reduce the gap between these two extreme setups. Recently, contributions following the numerical setup of one dimensional flame propagating in droplet mists coupled with the detailed description of the chemistry have been increasing in the literature, e.g. [2, 24, 29–33]. Although the geometrical simplifications are clear in such a numerical setup, it allows a good adherence with experimental measurements as shown in [24]. Further, such a setup is quite effective for the evaluation of parametric variations in ambient conditions (e.g. temperature and pressure) and the characteristics of the two-phase flow (e.g. initial droplet diameter, gas and liquid composition).

This work presents numerical simulations of flames propagating in droplet mists to further investigate the impacts of the multi-component description of droplets in reacting flows. In contrast to previous studies, this work considers a rigorous modeling approach [1] for the heat and mass transfer on droplets, which can accurately describe the energy and the mass transport of hydrophilic and non-hydrophilic fuels. Effects of liquid composition and the consideration of air humidity are systematically analyzed for different equivalence ratios.

The paper is structured as follows. After this introduction, modeling approaches are concisely described. Results are presented first focusing on the impact of air humidity, and then on the water addition in the fuel. The paper ends with conclusions.

2. Modeling approaches

The one-dimensional reacting flow solver CHEM1D [34] was used for the numerical simulations. It has been extended with a Lagrangian spray solver to study flames propagating in fuel and non-fuel droplet mists [30, 31, 33]. Simulations of unstrained laminar flames propagating in mono-dispersed isotropic sprays are presented in this manuscript, similarly to [2, 24, 29–33]. In the following, the resolved equations are briefly presented.

2.1. Gas Phase

The description of the carrier phase follows a variable-density low Mach number formulation. Following the strategies presented in [30, 33–36], the set of equations employed here is

$$\frac{d\dot{m}}{dx} = \sum_k S_k, \tag{1}$$

$$\frac{d(\dot{m}Y_i)}{dx} - \frac{d}{dx}\left(\rho Y_i V_i\right) = \dot{\omega}_i + \delta_{ik} S_k, \tag{2}$$

$$\frac{d(\dot{m}h)}{dx} = -\frac{d}{dx}\left[-\lambda\frac{dT}{dx} + \rho\sum_{i=1}^{N} Y_i h_i V_i - RT\sum_{i=1}^{N}\frac{D_i^T}{X_i M_i}\frac{dX_i}{dx}\right] + S_\mathrm{h}, \tag{3}$$

where $\dot{m} = \rho u$ is the mixture mass flux, x is the spatial coordinate, and S_k is the source term of vapor species k. Y_i is the mass fraction of the species $i \in [1, N_s - 1]$, N_s is the total number of species, V_i is the diffusion velocity, $\dot{\omega}_i$ is the reaction rate, and δ_{ik} is the Kronecker delta. h is the absolute enthalpy, h_i is the absolute enthalpy of each transported species i, while S_{h} denotes the coupling term between phases. The first term on the RHS of Eq. 3 refers to the heat flux, in which λ is the thermal conductivity, T is the temperature, R is the gas constant, D_i^T is the thermal diffusion coefficient, X is the molar fraction, and M is the molar mass. The computation of the diffusion coefficients ($D_{i,m}$ and D_i^T) is performed following Ern and Giovangigli [37].

To account for the chemical reactions, the mechanism proposed by [38] has been employed. It describes the oxidation of ethanol in air by means of 57 species and 379 intermediate reactions.

2.2. Liquid Phase

Since multi-component droplets are accounted for, the main changes in the liquid phase modeling compared to the previous works [30, 31, 33] refer to the heat and mass transfer. Herein, the model of [1] is applied, which accounts for the differential diffusion of vapor into the gas phase [1]

Heat and mass transfer on a droplet are given by

$$\dot{q}_d = 4\pi R\lambda \frac{Nu}{2}(T_\infty - T_s) + \sum_k \dot{m}_{d,k} L_k, \qquad \dot{m}_d = -4\pi R_d \rho D_k \frac{Sh_k}{2} B_{M,k}. \tag{4}$$

where $\dot{q}_d$ is the heat transfer rate, R_d the droplet radius, λ the heat conductivity of the gaseous mixture, Nu the Nusselt number, $\dot{m}_d$ the mass transfer rate, $\dot{m}_{d,k}$ the mass transfer rate of vapor species k, L_k the vaporization enthalpy of species k, ρ the mixture density, D_k the multi-component diffusion coefficient, and Sh_k the Sherwood number of vapor species k. Subscript s refers to quantities evaluated at the droplet surface. By adopting uniform temperature and composition in the droplet interior $\dot{q}_d = m_d \left(\sum_k Y_{L,k} c_{L,k}\right) dT_d/dt$, where $Y_{L,k}$ the liquid mass fraction and $c_{L,k}$ is the liquid specific heat of vapor species k. Following [5], a general approach is to consider that

$$Nu = \frac{\ln|B_T + 1|}{B_T} Nu^0, \qquad Sh_k = \frac{\ln\left|B_{M,k} + 1\right|}{B_{M,k}} Sh_k^0, \tag{5}$$

$$Nu^0 = 2 + 0.57 Re^{1/2} Pr^{1/3}, \qquad Sh_k^0 = 2 + 0.57 Re^{1/2} {Sc_k}^{1/3}, \tag{6}$$

where Nu^0 refers to empirical correlations derived from non-evaporating moving droplets, and Sh_k^0 is its analogous for mass transfer (see Eq. 6). $Re = \rho|u_\infty - u_d|d/\mu$ is the Reynolds number, u_∞ the bulk flow velocity, u_d and d the droplet velocity and diameter, μ the dynamic viscosity, Pr the Prandtl number, and $Sc_k = \mu/\rho D_k$ the species k Schmidt number. B_T and $B_{M,k}$ are the Spalding numbers for energy and species k:

$$B_T = \frac{(T_\infty - T_s)\sum_k c_{p,k}\dot{m}_{d,k}}{\dot{q}_d - \sum_k \dot{m}_{d,k} L_k}, \qquad B_{M,k} = \frac{\dot{m}_d Y_{k,s} - \dot{m}_d Y_{k,\infty}}{\dot{m}_{d,k} - \dot{m}_d Y_{k,s}}. \tag{7}$$

[1] In [4], it has been shown that this mode degenerates to the one of Abramzon and Sirignano [39]. In this way, a single approach is sufficient to conduct simulations for both multi- and single-component scenarios.

The multi-component diffusion coefficient D_k is computed with the Wilke approach [40], as in [1, 4]. Binary diffusion coefficients are computed with the Fuller-Giddings method [41]. For all simulations conducted with the MC approach, non-ideal VLE is accounted using the van Laar model [42]. The surrounding gas properties used for droplet phase change (i.e., μ, λ, c_p, and D_{ij}) are computed following [31], where the gas composition in the far field follows the species diluted approach (SD) including all participating species. The procedure adopted to couple both phases is detailed in [30], which has been straightforwardly extended to multi-component mists.

3. Results

Results are presented in two sections. The focus is on the laminar flame speed, a major quantity for turbulent flame modeling, and on the influence of the multi-component modeling on this quantity. The first one is concentrated on the impacts of the multi-component modeling on flames propagating in droplets mists of pure hydrophilic fuel in humid or dry air. The second one investigates the consequences of considering droplets composed of a mixture of this fuel and water for flames propagating in sprays.

Droplets are injected 30 mm upstream of the flame front with an initial diameter (d_0) of 50 μm. Variations of initial droplet diameter have been investigated previously in [30, 31, 33] for single-component fuel and non-fuel droplets. Herein, the initial droplet size has been selected as an intermediate value between small droplets < 25 μm, which predominantly interact with the flame pre-heating zone, and large ones > 75 μm, which respectively tend to penetrate far into the flame oxidation zone. The one-dimensional computational domain extends from -100 mm to 400 mm, in which the flame front is held at the coordinate 0.0 mm[2]. By setting an overall equivalence ratio ϕ_{over}, the mass flow of liquid is adjusted accordingly [30]. In all simulated cases, the inlet and initial droplet temperatures are 298 K [3]. Here, humid air refers to 100% relative humidity, i.e. $X_{H_2O} = 0.032$ at 298 K. Finally, results are presented for different ϕ_{over}, which refer to the overall equivalence ratio, i.e. the equivalent ϕ to when the spray is completely pre-vaporized.

3.1. Pure hydrophilic fuel droplet in humid air

The laminar flame speeds of spray flames in humid and dry air are presented in Fig. 1. Single-phase laminar flame speeds are also included for reference in both conditions, i.e. humid and dry air. The general trends are consistent with the literature (e.g. [24, 29, 31, 33]). Here, the focus is on the behaviors observed among the different modeling assumptions under various conditions. A specific discussion about the faster flames observed for two-phase flows when compared with single-phase (SP) ones is conducted in the Appendix A, where a novel justification for this phenomenon is presented.

Focusing first on the SC results, as it occurs for single-phase flames, the inclusion of water vapor into the air stream leads to lower flame speed values compared to the results achieved with

[2]The flame front position is where the gas temperature is increased by 200 K compared to the inlet temperature.

[3]It must be remembered that the mixture's absolute enthalpy differs between SP and spray cases. The evaporating cooling induced by the spray has been shown to decrease the flame speed in [30], and this trend must be kept in mind in the comparison between gaseous and spray cases.

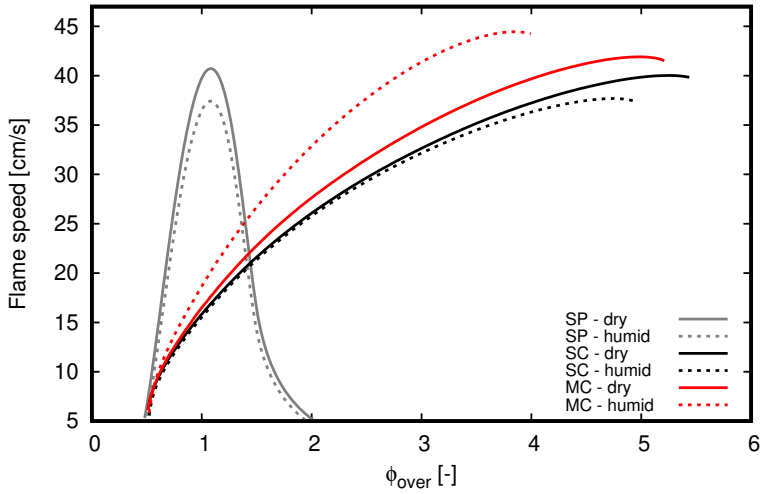

Figure 1: Laminar flame speed by equivalence ratio of single phase (SP) and two-phase freely propagating flames for both humid and dry air. In all mists pure ethanol is injected. SC denotes single component and MC multi component droplet model.

dry air. The consideration of this reaction product already in the reactants stream may also justify the anticipation of the quenching point to lower values of ϕ_{over}, when compared with the dry air cases. However, the deviations between both SC cases are to be noticed. They increase as ϕ_{over} increases, which is counter-intuitive, as less vapor is proportionally found in rich mixtures than in lean ones. Nevertheless, this characteristic resembles what is observed for the fastest SP flames. According to Liang et al. [43], the chemical kinetic effects of water addition over the single-phase laminar flame speed are very small compared to thermophysical effects, so the explanation must be found in the latter option.

The importance of the consideration of a multi-component (MC) approach to describe hydrophilic fuel droplets is clearly evident in Fig. 1. By comparing SC and MC cases in dry air, flame speeds with the MC approach are always faster than with the SC simplification. Deviations increase as ϕ_{over} increases to approximately 10%. By considering the MC approach, the water formed during the combustion reaction is allowed to interact with the hydrophilic droplets[4]. Although a non-ideal VLE model is applied, droplet temperatures are bounded by the boiling point temperatures of individual components, i.e. $T_{b,\text{C}_2\text{H}_5\text{OH}} = 351.5\ K$ and $T_{b,\text{H}_2\text{O}} = 373.2\ K$. Hence, when droplets do not evaporate before reaching the reaction zone, a cold liquid structure interacts with the flame. When the MC approach is turned on, water formed in the combustion process is able to condensate on the droplet surface, releasing heat to heat up both gaseous and liquid phases.

Water condensation on droplets surfaces was predicted before starting this study, but such an impact on flame speeds was unexpected. These results are clearly novel, but not as intriguing as those seen in Fig. 1 for the MC approach in humid atmospheres. As observed for SP cases and those of two-phase flows using the SC approach, by adding humidity, the laminar flame speed decreases for the entire ϕ_{over} span. In contrast, the inclusion of humidity when modeling droplets

[4]In the SC approach, the droplet composition is fixed to a single species.

with an MC approach, the flame propagation becomes clearly faster as ϕ_{over} increases. Flames are about 20% faster than those computed in dry air. In humid air, the differences are even larger between MC and SC, but what is more intriguing is the totally different behaviors when adding humidity: while humid air leads to slightly decreased flame speeds in the SC approach, there is a very strong increase in flame speed in the MC approach, with almost 20% faster flames.

To investigate these behaviors, Ethanol and water mass fractions profiles of the gaseous mixture are presented with the gas temperature of flames for $\phi_{\text{over}} = 3.0$ in Fig. 2. When focusing on the dry air scenario, the presented profiles are close to each other. Some deviations are easier to be noticed in the Y_{H_2O} profiles, in which the MC case depicts lower values of this quantity in the region where droplets penetrate into the oxidation zone (see Fig. 3). Such lower values indicate that water vapor formed by combustion reactions condensates on droplet surfaces if the MC description is enabled. The condensation is confirmed through the profiles of liquid mass fractions and the coupling source terms presented in Figs. 3 and 4. Due to the exothermic characteristic of the condensation mechanism, the temperature of both gaseous and liquid phases increases. Although minimal, this can already be noticed in the gas temperature for the dry air scenario by comparing MC and SC cases, but it is clearly more pronounced in the humid air scenario. On the other hand, the increase of the droplet temperature is evident in Fig. 3 for both scenarios. Such a heat transfer caused by the condensation mechanism, which is consequently induced by the hydrophilic nature of the fuel, partially justifies the higher flame speed values indicated in Fig. 1.

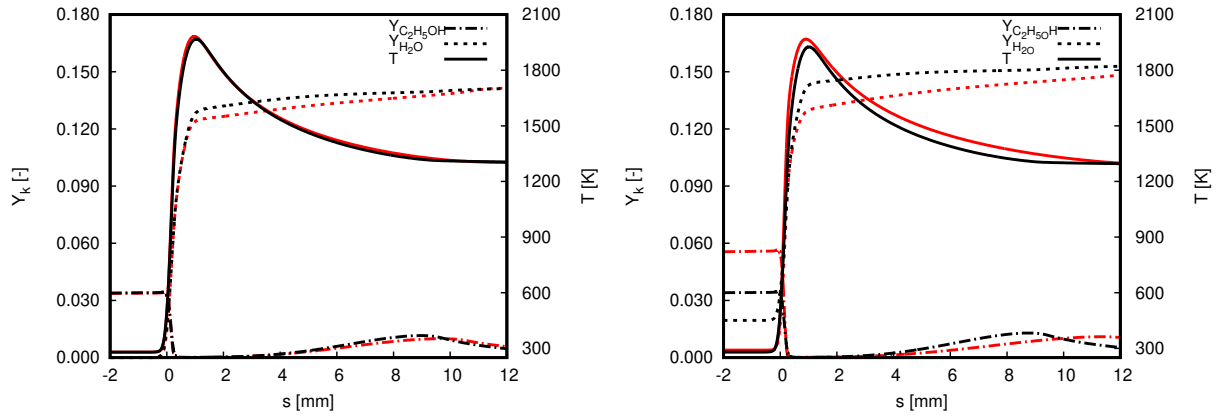

Figure 2: Evolution of the gas temperature and the mass fractions of ethanol and water. On the left: dry air; on the right: humid air. SC: black; MC: red.

No differences in ethanol profiles are noticed at the pre-vaporization zone in Fig. 2 for dry air. This is expected since droplet and gas compositions are the same in this region. However, far into the reaction zone, ethanol emerges in both flames. Differences between both cases in dry air are justified by the late injection of the remaining ethanol by MC droplets (see $S_{C_2H_5OH}$ profile in Fig. 4), which do also penetrate farther into the flame (see Fig. 3).

When comparing both scenarios, deviations in humid air are much more evident than those of dry air. Except for $Y_{C_2H_5OH}$ and Y_{H_2O} profiles, the general behaviors seen for dry air are maintained for humid air. Both ethanol and water profiles change in the pre-vaporization zone between approaches because of the interaction of the hydrophilic droplets with the air humidity when en-

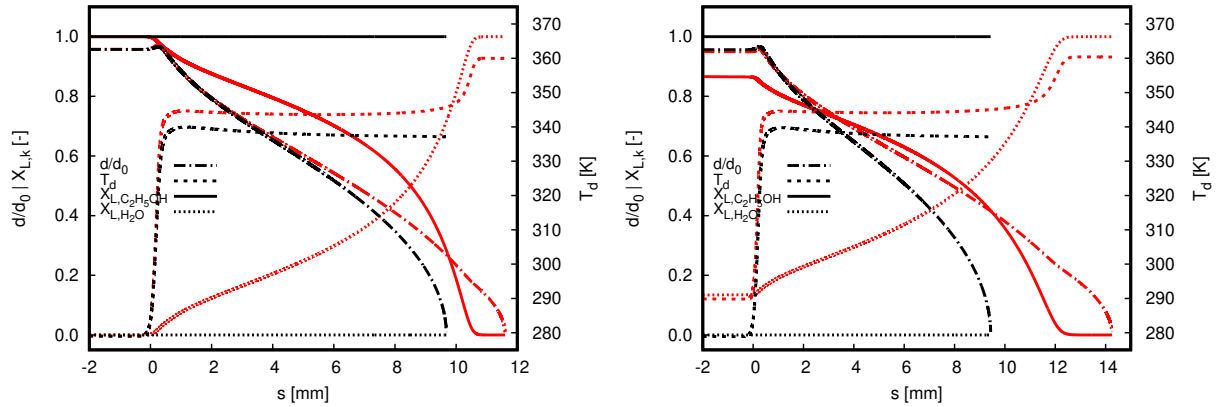

Figure 3: Evolution of the normalized droplet diameter, droplet temperature and the liquid mass fractions of ethanol and water. On the left: dry air; on the right: humid air. SC: black; MC: red.

abling the MC model. Accordingly, the ethanol mass fraction and gas and droplet temperatures reaching the flame are higher with the MC approach. In contrast, water mass fraction arriving at the reaction zone is lower with the MC approach.

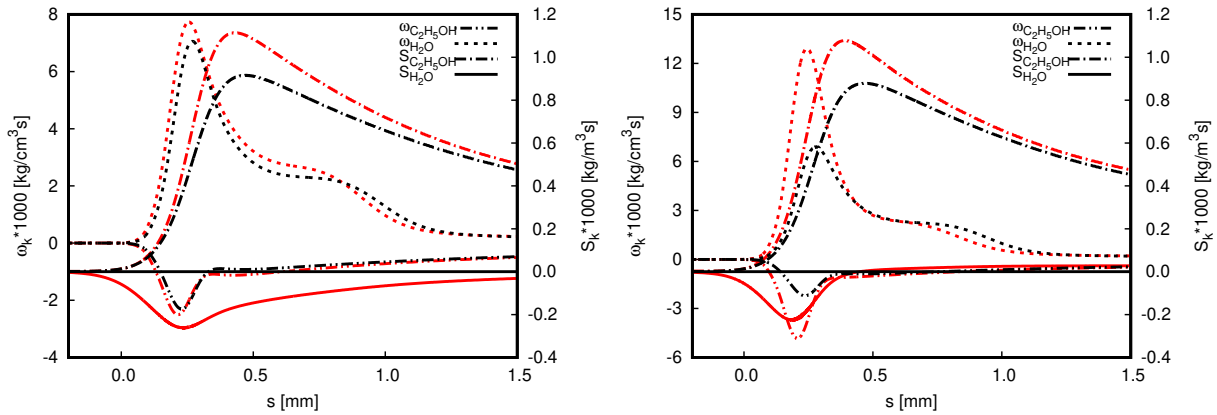

Figure 4: Evolution of reaction source terms $\dot{\omega}_k$ and coupling source terms S_k for ethanol and water. On the left: dry air; on the right: humid air. SC: black; MC: red.

The most important phenomenon observed in Fig. 4 refers to the higher values of $S_{C_2H_5OH}$ in the reaction zone for the MC when compared with the SC approach for both dry and humid air. This shows that water condensation enhances ethanol evaporation, which can be justified by the droplet heat-up and droplet compositions change as depicted in Fig. 3. The intensification of the ethanol evaporation by enabling the MC approach occurs as soon as water starts to be formed in the flame, which coincides with the reaction zone. As a consequence, fuel is directly injected into the high reaction rates region, intensifying them and allowing for an increase in the flame propagation velocity. The alignment between $\omega_{C_2H_5OH}$ and chemical heat release rate (HRR) profiles presented respectively in Figs. 4 and 5 corroborates this rationale. Concerning the scenario with humid air, the HRR profile is slightly anticipated when compared with its counterpart for both flames

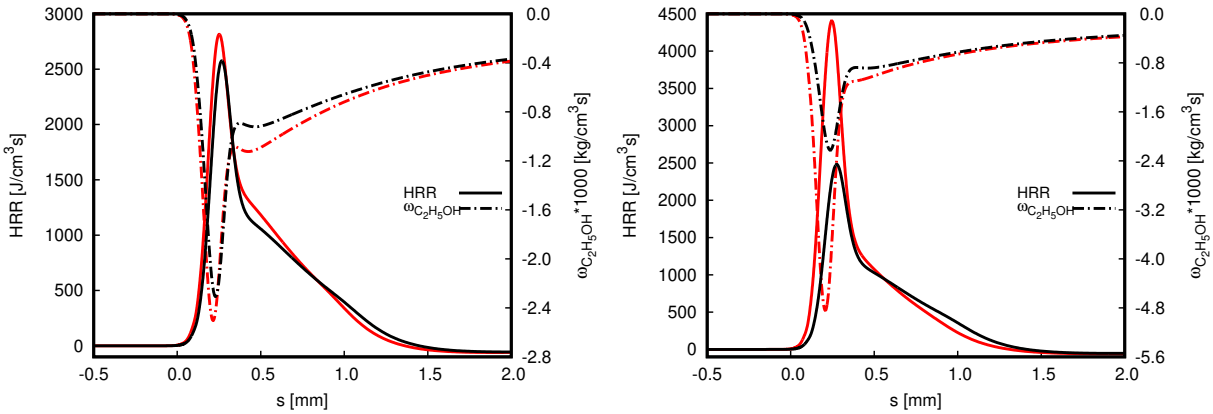

Figure 5: Evolution of the heat release rate (HRR) and the chemical source term of ethanol $\omega_{C_2H_5OH}$. On the left: dry air; on the right: humid air. SC: black; MC: red.

computed with the MC approach. This occurs because of the higher mass fractions of ethanol reaching the flame front when water condensation occurs already in the pre-vaporization zone.

So far, analyses are concentrated for a single value of the overall equivalence ratio, i.e. $\phi_{over} = 3.0$, since deviations among scenarios are more pronounced for rich mixtures. Nevertheless, such discussions are valid throughout the computed span of ϕ_{over}. To demonstrate this, Figs. 6, 7, and 8 present colormaps of selected quantities. Such colormaps were constructed with the computed flames in a grid defined by ϕ_{over} and the spatial coordinate x.

In Figs. 6 and 7 selected quantities from flames computed in both scenarios with dry air are presented and compared using deviation plots. To compute such deviations, the following expression is used $\epsilon_\psi = \psi - \psi_{ref}$, where ψ refers to the compared quantity and subscripts $_{ref}$ to a reference value, i.e. the quantity presented on the left in the colormap figures.

Gas and droplet temperatures and the mass fraction of water show a similar behavior previously noted in profile plots. As the values of ϕ_{over} increase, droplet penetration increases, and the behavior noticed for gas and droplet temperatures at $\phi_{over} = 3.0$ is replicated. However, the evolution of Y_{H_2O} do not follow a regular shape throughout ϕ_{over}. From results achieved for both SC and MC approaches, Y_{H_2O} profiles depict a monotonic behavior through x up to $\phi_{over} \approx 3.0$. Around this value of ϕ_{over}, the mass fraction of water reaches a maximum. But, for mixtures richer than $\phi_{over} \approx 3.0$, the Y_{H_2O} reaches a maximum between 0mm and 10mm, then slowly decreases. This occurs due to the high penetration of the droplet into the oxidation zone and the late injection of fuel and absorption of water in MC cases, as noticed through the $Y_{C_2H_5OH}$ profiles in Fig. 8 [5].

The remaining key quantities used to justify the flame speed behavior in the different scenarios are presented in Fig. 7. The coupling source terms follow the trend noticed in the profile plots. Throughout the ϕ_{over} no shape changes are noticed, but values are higher for cases computed with the MC approach. In contrast, the remaining source terms in Fig. 7 do not show such a regular behavior. From the leanest to the highest ϕ_{over}, the negative peak values of $\dot{\omega}_{C_2H_5OH}$ regularly approach to the position 0.0 mm and become more intense. Such a behavior is maintained

[5] Notice that colormaps of the MC computation in humid air are plotted in both Figs. 6 and 8.

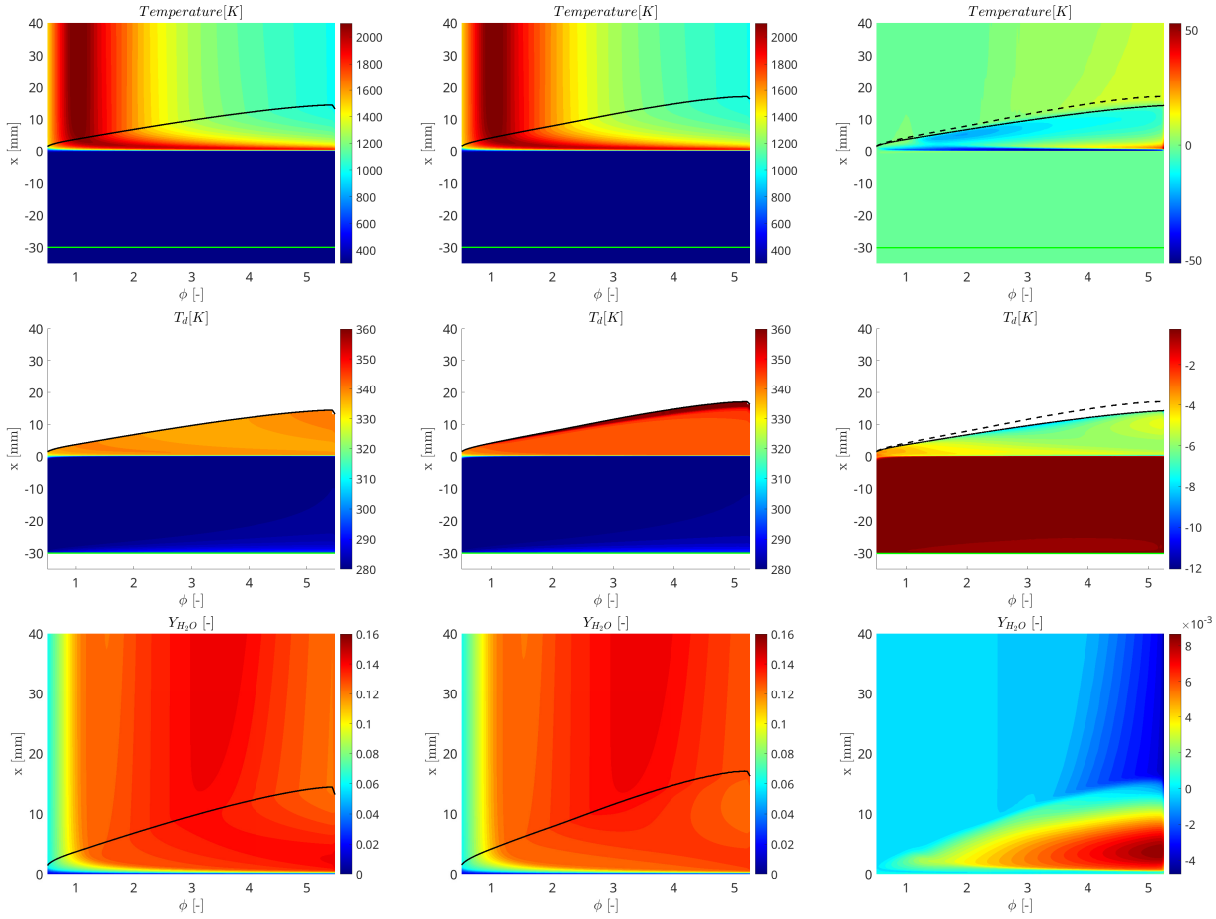

Figure 6: Colormaps of selected quantities of flames computed with the SC and the MC approaches in dry air. Left: SC; middle: MC; right: deviations between SC and MC approaches. Black line: penetration threshold; green line: droplet injection position; dashed line: penetration threshold for humid air in deviation plots.

until $\phi_{\text{over}} \approx 2.5$ is reached. For richer mixtures, a second one appears downstream of the first $\dot{\omega}_{C_2H_5OH}$ negative peak, indicating the decomposition of the later released ethanol by droplets into the oxidation zone. Despite this bimodal shape of $\dot{\omega}_{C_2H_5OH}$ through x, the HRR profiles become gradually more concentrated and intense as ϕ_{over} becomes higher until the corresponding value of the maximum laminar flame speed is reached. The HRR slowly decreases for richer mixtures until the quenching point is reached. Altogether, the colormaps presented in Figs. 6 and 7 attest the reasoning presented in terms of profile plots to justify the flame speed behavior noticed in Fig. 1 when including or neglecting the MC description of hydrophilic fuels.

This section is closed by discussing the colormaps of selected quantities that are more pertinent when the MC description is enabled, in Fig. 8. The impacts of considering air humidity are clearly noticed in $Y_{C_2H_5OH}$ in Fig. 8. As with profile plots, water in the fresh reactants intensifies the pre-vaporization of ethanol. This phenomenon increases with ϕ_{over}, corroborating the justification given to the increase of the flame speed as the mixture becomes richer. Also, in $Y_{C_2H_5OH}$ colormaps, as the pre-vaporization increases, less ethanol is available in the droplets and the amount of ethanol

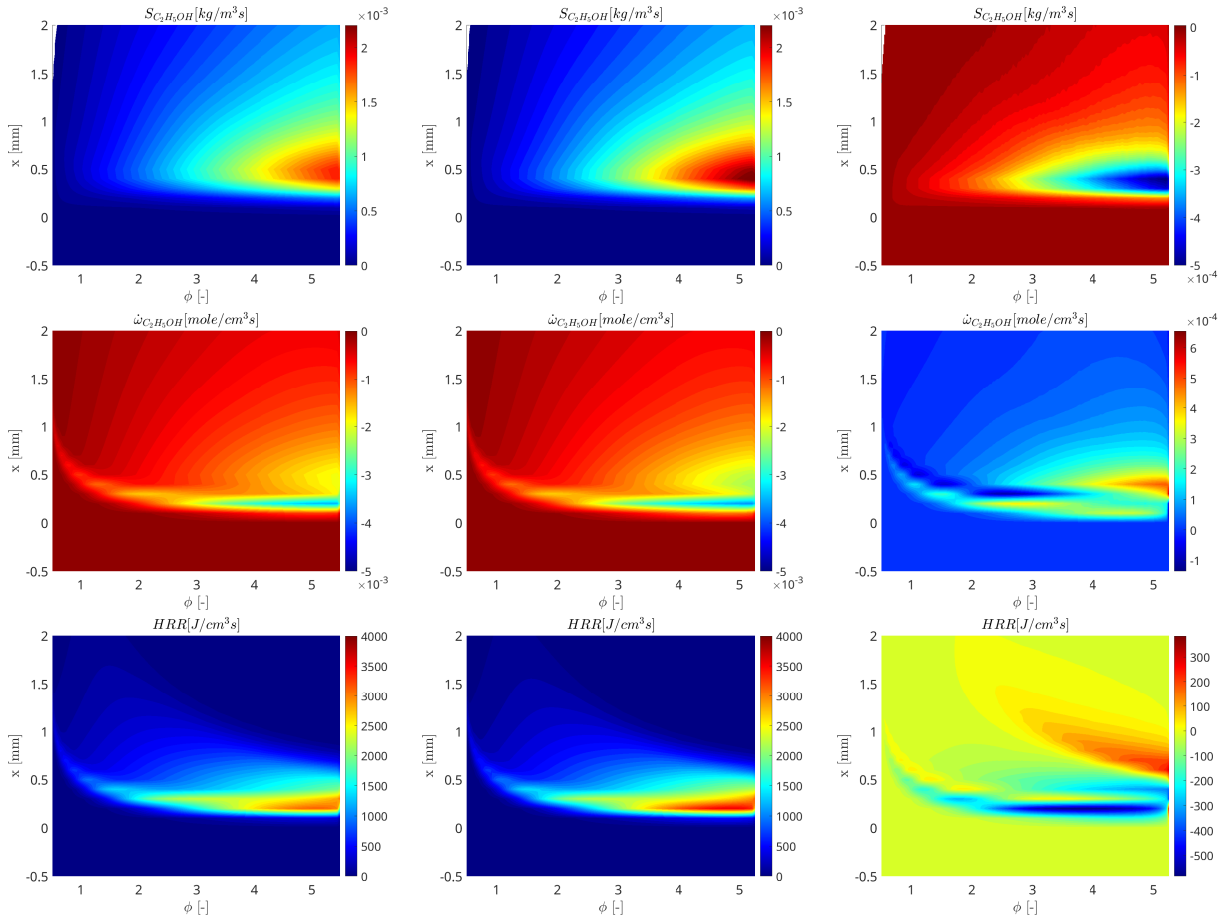

Figure 7: Colormaps of selected source terms of flames computed with the SC and the MC approaches in dry air. Left: SC; middle: MC; right: deviations between SC and MC approaches.

released in the oxidation zone decreases. The corresponding change in droplet composition is reported in terms of the liquid molar fraction of fuel in the second row of Fig. 8. As a droplet moves through the flame, its composition changes from pure fuel to pure water. The presence of air humidity accelerates this process and, in this scenario, droplets interacting with flames have a higher amount of water. Further, droplets in humid air penetrate more into the oxidation zone than droplets in dry air, due to the lowers evaporation rate of water. Regarding X_{L,C_2H_5OH}, the variation from lean to rich mixtures is obviously due to the increase in ϕ_{over}. Very interestingly, we notice that the available ethanol at the flame location is increasing with ϕ_{over}. It confirms that pre-vaporization is a first source of flame speed increase, as more gaseous fuel is immediately available to feed the flame.

Another important quantity to be tracked in MC scenarios is the coupling source term of water S_{H_2O}. By comparing humid and dry air scenarios, water starts to condense as soon as droplets are injected into a humid atmosphere. Since no water is available in the pre-vaporization zone with dry air, S_{H_2O} is zero in this region. However, the more intense values of S_{H_2O} occur in the reaction zone for both cases, which are focused in Fig. 8. This is more pronounced as ϕ_{over} increases.

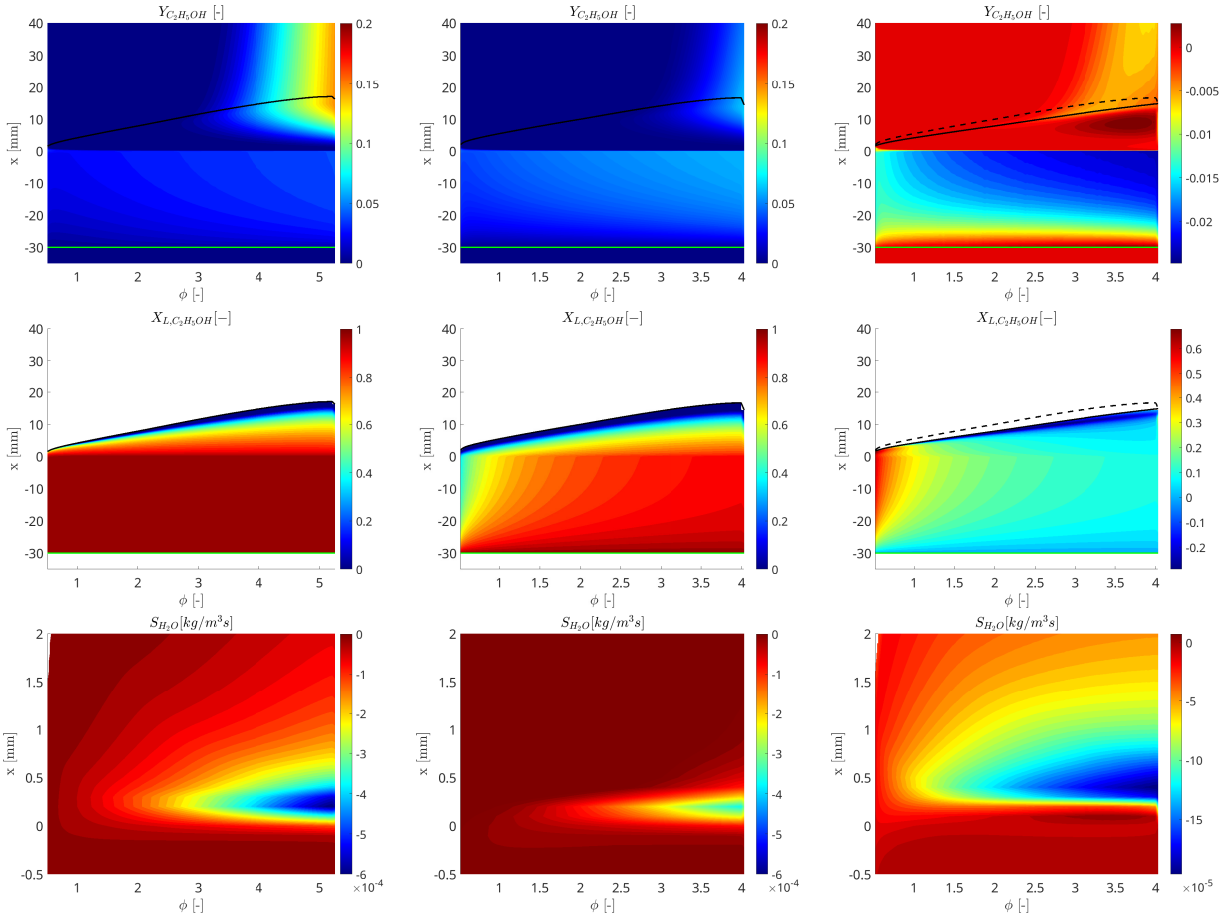

Figure 8: Colormaps of selected quantities of flames computed with the MC approach in dry and humid air. Left: dry air; middle: humid air; right: deviations between flames in dry and humid air. Black line: penetration threshold; green line: droplet injection position; dashed line: penetration threshold for humid air in deviation plots.

Further deviations are noticed in the oxidation zone due to the contrasting droplet compositions. In humid air scenarios, high values of $S_{\mathrm{H_2O}}$ in the oxidation zone indicate the late release of water vapor caused by the higher $X_{L,\mathrm{H_2O}}$ values.

3.2. Analysis of hydrous ethanol

Following the investigation of pure hydrophilic fuel droplets interacting with flames, it is a natural choice to analyze how such an interaction evolves for multi-component droplets composed by the hydrophilic fuel and water. Throughout this section, droplets are composed of binary mixtures of ethanol and water, i.e. 92.5% of ethanol and 7.5% of water in mass, following the composition of hydrous ethanol with higher percentage of water specified in [44].

Laminar flame speeds are presented in Fig. 9 against ϕ_{over}, in humid and in dry air. In contrast to Fig. 1, the influence of mixing water with fuel in the liquid phase follows the expected trend: the hydrous ethanol delivers lower flame speed values than the corresponding cases of pure ethanol. However, the influence of air humidity follows the same trends previously noticed for pure ethanol.

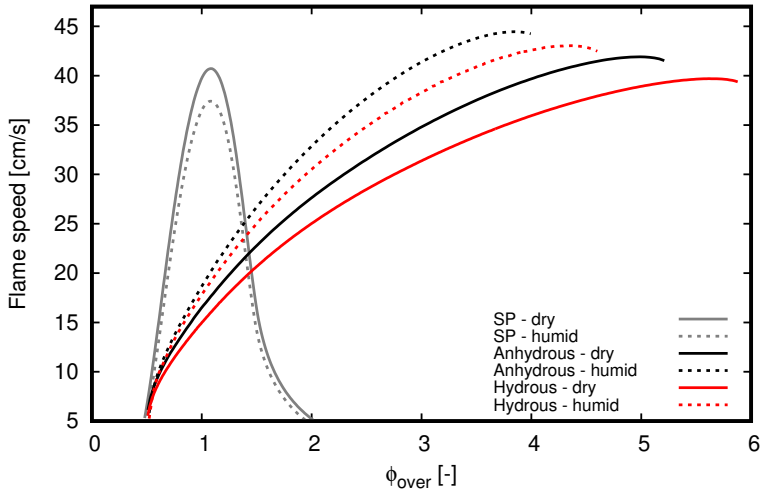

Figure 9: Laminar flame speed by equivalence ratio of single phase (SP) and two-phase freely propagating flames for both humid and dry air. In all mists the MC approach is applied.

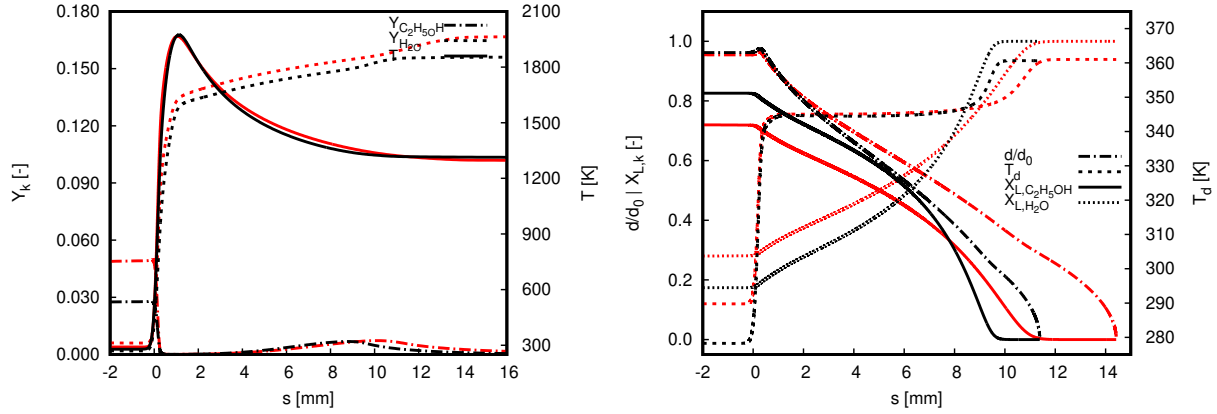

Figure 10: Evolution of carrier and dispersed phase quantities. Black: dry air; red: humid air.

Figures 10 and 11 present profiles plots for $\phi_{\text{over}} = 3.0$ of the same quantities as in Sec. 3.1. In view of the quantities used to justify the flame speed, differences between cases computed with hydrous ethanol in dry and humid air are more pronounced for gaseous mass fractions, liquid molar fractions, reaction rates, and HRR. The intensification of the flame speed values from dry to humid air as seen in Fig. 9 for hydrous ethanol cases can be justified by the higher mass fraction of ethanol arriving at the flame front. The higher release of ethanol vapor into the reaction zone does occur, but is less pronounced than the pre-vaporization of ethanol before reaching the flame. Accordingly, it is expected that, by reducing the droplet injection distance, flame speed values computed in dry and humid atmospheres will approach each other. However, the minimal evaporation of fuel in the pre-vaporization zone and the higher release of fuel vapor straight into the reaction zone shall preserve higher flame speed values for cases computed in humid air.

The composition of the hydrous ethanol droplets, typical for commercial fuels in Brazil, might

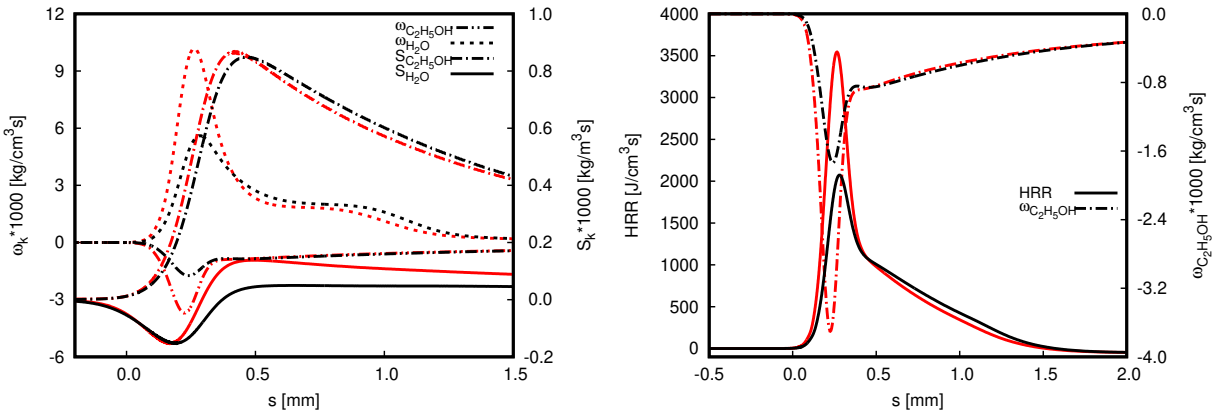

Figure 11: Evolution of selected source terms. Black: dry air; red: humid air.

generate the so-called inversion problem, first documented in [1] and where the less volatile component leaves the droplet first. Simulations conducted in [1] are performed for single droplets in atmospheres with fixed or varying composition, not modified by the vapor released or collected by droplets. Within that context, it was possible to observe for binary droplets of alcohols and water that water completely left the droplet first. This phenomenon is suppressed by including minimal water vapor in the far-field gas. The required amount depends on the liquid composition, initial gas and liquid temperatures, and VLE and vapor pressure modeling approaches. In the present work and following the procedure applied in [1] for a fixed far field gas composition and temperature of 298K at 101.325kPa, the inversion problem is suppressed for the chosen hydrous ethanol composition for a relative humidity higher than 1.5%, i.e. $Y_{\mathrm{H_2O}} = 0.0003$. Here, the small amount of water released by droplets in the near field of the injection allows a value of $Y_{\mathrm{H_2O}} > 0.0003$. As a result, the inversion problem is suppressed, and the evolution of $X_{L,\mathrm{H_2O}}$ presented in Figs. 10 and 12 show that water is the last component remaining in both conditions dry and humid air.

The results presented in Fig. 12 clearly indicate that penetration is farther into the flame for cases computed with humid air. This behavior agrees with the previously reported results for anhydrous ethanol. The water mass fraction and liquid molar fraction colormaps clearly point out that the interaction of droplets and the air humidity in the pre-vaporization zone are the main source of deviation between both scenarios. In humid air simulations, droplets arrive at the flames with more water. Consequently, the overall evaporation rate reduces, and droplets penetrate farther in the oxidation zone. The contour plots of the coupling source term $S_{\mathrm{H_2O}}$ point out the differences between both scenarios. As no humidity is present in the pre-vaporization zone of the dry air simulations, this term is slightly positive for $x < 0.0$. As droplets start to interact with the flame, strong condensation occurs, since $S_{\mathrm{H_2O}} < 0$. A rapid inversion to an evaporation mode ($S_{\mathrm{H_2O}} > 0$) follows as the right temperatures of the gas phase shift droplets temperature to a plateau (see Fig. 10), consequently indicating that both ethanol and water are leaving the droplets. For the colormaps of $\dot{\omega}_{\mathrm{H_2O}}$ and HRR, both depict similar behaviors. Values become more intense and concentrated with ϕ_{over} in a straight zone from 0.0mm to 1.0mm. Although simulations with dry air allow a larger span of ϕ_{over}, values of both $\dot{\omega}_{\mathrm{H_2O}}$ and HRR are predominantly more intense for the humid air case. In summary, the results presented in Fig. 8 corroborate the reasoning presented

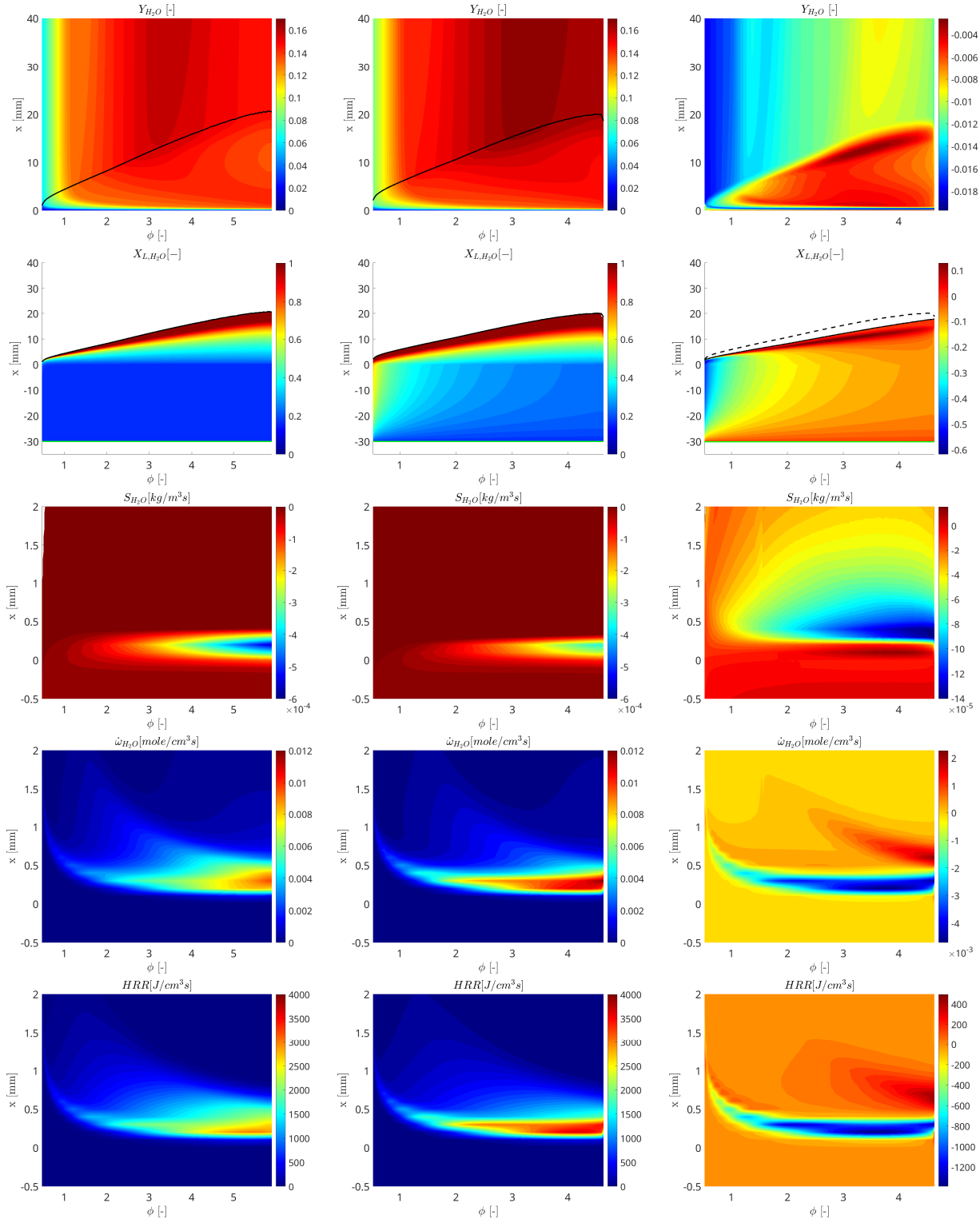

Figure 12: Colormaps of selected quantities of flames computed with hydrous ethanol in dry and humid air. Left: dry air; middle: humid air; right: deviations between flames in dry and humid air. Black line: penetration threshold; green line: droplet injection position; dashed line: penetration threshold for humid air in deviation plots.

regarding profile plots to justify the higher flame speed achieved in humid rather than dry air.

4. Conclusions

Flames propagating in droplet mists were simulated with a detailed description of the chemistry and the diffusion transport for different hydrophilic fuel compositions to clearly pose the importance of considering the multi-component description of liquid fuels. Analyses systematically evolved from single to two-phase flows and from single to multi-component modeling approaches. To rigorously account for the differential diffusion of vapor into the gas flow, the approach in [14] has been applied. Novel and impactful findings have been obtained regarding flame speed, which were carefully justified throughout the manuscript. In addition, a novel justification was presented for the observed higher flame speed values of flames propagating in droplets mists when compared to single phase flames. The results show that the description of a hydrophilic liquid as a single-component substance suppresses the description of important phenomena for reacting two-phase flows.

Results were first concentrated on simulations of flames propagating in sprays of pure hydrophilic fuel. Therein, intriguing findings were noticed. As soon as the multi-component approach is enabled, flame speeds become higher than those values achieved with the single-component approach. Even more intriguing was the inverse behavior of the flame speed values when computations were performed in humid air. Instead of being reduced, as for single phase or in mists with the single component approach, flames propagates faster by including multi-component phenomena. These phenomena could be properly justified by the detailed description of each species' heat and mass transfer mechanisms, as allowed by the chosen modeling strategy.

Then, investigations of flames propagating in droplet mists formed by binary mixtures of ethanol and water are conducted. Typically, behaviors noticed for pure ethanol droplets are reproduced for hydrous ethanol. Nevertheless, flame speeds are lower than those obtained with pure ethanol droplets given a specific atmosphere. Special attention has been paid to the occurrence of the so-called inversion problem, noticed in [1]. However, the two-way coupling, included for the first time with the approach proposed in [14], inhibits such a phenomenon for the simulated setups, as water vapor becomes present in the far field.

The present study is an important contribution to the technological development associated with using biofuels and sustainable aviation fuels (SAF). A special focus was given to ethanol due to its increasing usage for transportation. However, other alcohols, such as methanol, and ketones, are expected to demonstrate the same behavior because of their corresponding hydrophilic characteristic. Results indicate that air humidity does influence basic flame characteristics, which may support the development of strategies to control the combustion process better when using this kind of fuels. We highlight that the achieved results are not observed experimentally so far, as it is not a common practice to control air humidity in reacting flow investigations. Therefore, the achieved outcomes can be used as a motivation for subsequent experimental analyses.

Acknowledgements

We acknowledge the financial support from São Paulo Research Foundation (FAPESP - grant # 2021/14245-1). The support of Fundação de Desenvolvimento da Pesquisa - Fundep, Rota 2030

- Linha V and Coordenação de Aperfeiçoamento de Pessoal de Nível Superior – Brasil (CAPES) – Finance Code 001 are also acknowledge.

Appendix A. Explanation about faster flames encountered in spray combustion

Flames propagating in droplet mists show higher maximum values of the laminar flame speeds than flames in mixtures of gaseous reactants. This behavior occurs besides the higher absolute enthalpy of gaseous flames at similar overall equivalence ratios. This phenomenon was early noticed in experimental works (e.g. [45, 46]) and later reproduced numerically in one-dimensional flames described by detailed reaction mechanisms (e.g. [29, 30]). Although many rationales were used to explain such high flame speeds in the literature, none seems sufficient to justify it.

Different mathematical expressions are available to estimate the laminar flame speed (s_l) of gaseous flames (e.g. [47–49]). Kuehne et al. [50] present an equation which allows the computation of the consumption speed (s_c) in terms of the source term of a reaction progress variable $\dot{\omega}_{pv}$,

$$s_c \propto \int_{-\infty}^{\infty} \dot{\omega}_{pv} dx, \quad \text{in which} \quad s_l = s_c - u_u \tag{A.1}$$

and u_u refers to the unburnt gas velocity. Such an expression offers an advantage to analyze flames propagating in droplets mists, since according to the composition of the reaction progress variable (Y_{pv}), a phase coupling term can be avoided in its corresponding transport equation. As a result, a clearer connection between s_l and the integral of $\dot{\omega}_{pv}$ is noticed when compared with other expressions based on the integral of the HRR and the reaction rates (e.g. summarized in [33]), which accounts for coupling source terms. Results presented in Fig. A.13 demonstrates that the proportionality presented for gaseous flames in Eq. A.1 does also hold for flames propagating in droplets mists. Specifically, results presented in Fig. A.13 do not coincide with the previous ones presented throughout this manuscript due to the diffusion transport model chosen for the analysis presented in this section, as explained in what follows.

With this aspect in mind, during the development of the present work, some analyses have been conducted about the evolution of the spray flames in terms of the local mixture fraction (Z) and the reaction progress variable employed in [51], i.e. $Y_{pv} = Y_{\mathrm{CO_2}}/M_{\mathrm{CO_2}} + Y_{\mathrm{H_2O}}/2.5M_{\mathrm{H_2O}} + Y_{\mathrm{CO}}/1.5M_{\mathrm{CO}}$. In contrast to premixed gaseous flames, where only Y_{pv} varies for a fixed Z, there is a simultaneous evolution of Z and Y_{pv} in spray flames, due to the gradual release of vapor across the flame by droplets. This was previously discussed in [30] and is plotted in Fig. A.14 over a Flamelet Generated Manifold (FGM) colored by $\dot{\omega}_{pv}$. To allow a better approximation of the reaction stages among spray flames and the FGM depicted in Fig. A.14, the considered spray flames in this section do no account for the evaporative cooling effects (see [30]), but are based on the SC approach and the diffusion transport is modeled by the unity Lewis number strategy by enforcing that $Sc = Pr = 0.7$. The FGM was constructed with premixed gaseous flamelets computed with the mechanism proposed in [38] for $\phi \in [0.47, 1.97]$ following a similar strategy employed in [14]. The same diffusion transport approach applied for the spray flames are used to compute the premixed gaseous flamelets. As shown in [14], simulations conducted with, virtually, the same FGM table are able to recover the laminar flame speed of flames propagating in droplets

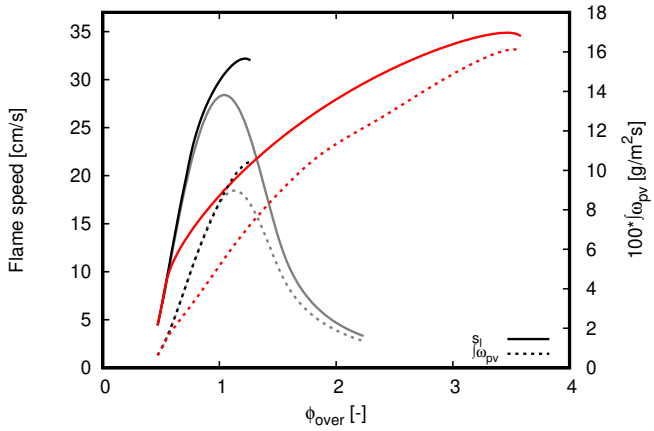

Figure A.13: Laminar flame speed and $\int_{-\infty}^{\infty} \dot{\omega}_{pv} dx$ by equivalence ratio of single phase (SP) freely propagating flames and flames propagating in droplets mists with $d_d^0 = 25\mu$m and $d_d^0 = 50\mu$m. Gray: SP; black: $d_d^0 = 25\mu$m; red: $d_d^0 = 50\mu$m.

mists for a range of ϕ_{over} and d_d^0. In Fig. A.14 the fastest flames found in Fig. A.13 respectively for the gaseous flames and those associated with the $d^0 = 25\ \mu$m and $d^0 = 50\ \mu$m mists.

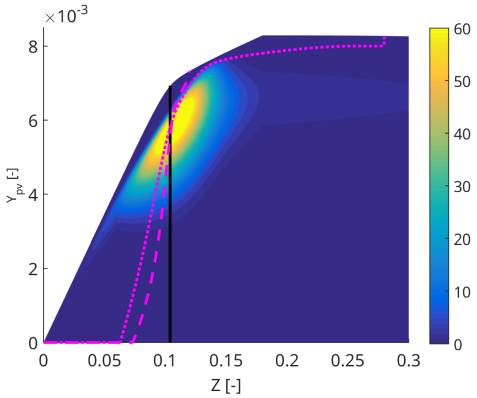

Figure A.14: Flame paths ploted over a Flamelet Generated Manifold colored by $\dot{\omega}_{pv}$. Black line refers to the fastest gaseous flame while magenta to flame propagating in droplet mists. Dashed line: $d_d^0 = 25\mu$m and dotted line: $d_d^0 = 50\mu$m.

By plotting the evolution of flames propagating in a droplet mists over a $\dot{\omega}_{pv}$ manifold on Z and Y_{pv}, it turns out that, according to the vapor release rate across the flame, reaction paths are able to cross a broader region of high values of $\dot{\omega}_{pv}$ when compared to premixed gaseous flames. As droplets mass transfer rates presents larger time scales than combustion reactions (e.g. [52–54]), it is possible to conclude that reaction paths do also stays longer in regions with high values of $\dot{\omega}_{pv}$. The results presented in Fig. A.15 corroborates this rationale. Figure A.15 presents profiles of $\dot{\omega}_{pv}$ and HRR for the three flames traced over the FGM in Fig. A.14. As noticed, the flames propagating in droplets mists depict broader regions where $\dot{\omega}_{pv} > 0$.

In conclusion, the distribution of fuel throughout the flame by the mass transfer among phases

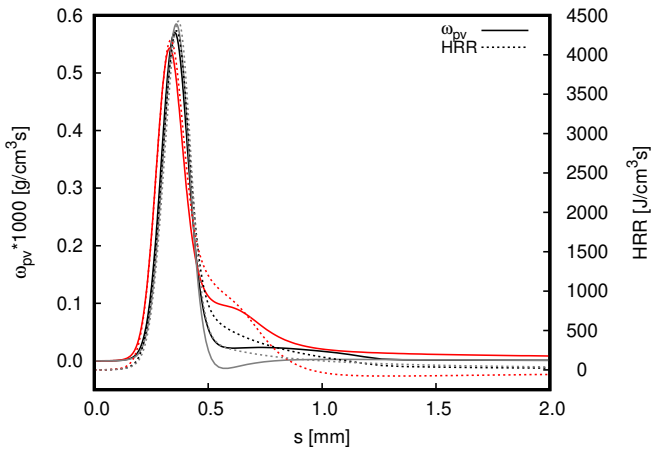

Figure A.15: Development of $\dot{\omega}_{pv}$ and HRR throughout the spacial coordinate x for the three flames traced over the FGM in Fig. A.14. Gray: SP; black: $d_d^0 = 25\mu$m; red: $d_d^0 = 50\mu$m.

allow an increase of the reaction rate which consequently impacts on the prediction of the flame speed. On one hand, in terms of a valid progress variable, the fuel injection in the carrier phase by the coupling source terms allows further formation of combustion products at high reaction rates, which is revealed by the continuous and distributed values of $\dot{\omega}_{pv}$ throughout the flame. On the other hand, the interaction of droplets and flames adds fuel enthalpy throughout the reaction zone, allowing the enhancement of the heat release rate within the reaction zone. As a result, flame speed is intensified when compared to gaseous combustion. This observation is not restricted to flames neglecting the evaporative cooling and it is not specific to a diffusion transport model.

References

[1] F. L. S. Filho, A. C. Santos, A. Vié, G. C. K. Filho, A new robust modeling strategy for multi-component droplet heat and mass transfer in general ambient conditions, Int. J. Heat Mass Transfer 194 (2022) 123102.

[2] V. Shastry, Q. Cazeres, B. Rochette, E. Riber, B. Cuenot, Numerical study of multicomponent spray flame propagation, Proc. Combust. Inst. 38 (2021) 3201–3211.

[3] M. Bonanni, M. Ihme, Interaction of preferential evaporation and low-temperature chemistry in multicomponent counterflow spray flames, Proc. Combust. Inst. (2022).

[4] A. C. Santos, F. L. S. Filho, A. Vié, The general formulation of the energy equation and the impact of enthalpy diffusion on multi-component droplet heat and mass transfer, Int. J. Heat Mass Transfer 210 (2023) 124172.

[5] S. S. Sazhin, Advanced models of fuel droplet heating and evaporation, Prog. Energy Comb. Sci. 32 (2006) 162–214.

[6] W. A. Sirignano, Fluid Dynamics and transport of droplets and sprays, 2nd ed., Cambridge University Press, 2010.

[7] V. Ebrahimian, C. Habchi, Towards a predictive evaporation model for multi-component hydrocarbon droplets at all pressure conditions, Int. J. Heat Mass Transfer 54 (2011) 3552–3565.

[8] L. Zhang, S. C. Kong, Multicomponent vaporization modeling of bio-oil and its mixtures with other fuels, Fuel 95 (2012) 471–480.

[9] S. Tonini, G. E. Cossali, An exact solution of the mass transport equations for spheroidal evaporating drops, Int. J. Heat Mass Transfer 60 (2013) 236–240.

[10] G. Lupo, C. Duwig, A numerical study of ethanol-water droplet evaporation, J. Eng. Gas Turbines Power 140 (2018) 21401.

[11] A. P. Pinheiro, O. Rybdylova, I. A. Zubrilin, S. S. Sazhin, F. L. S. Filho, J. M. Vedovotto, Modelling of aviation kerosene droplet heating and evaporation using complete fuel composition and surrogates, Fuel 305 (2021).
[12] P. Keller, A. Bader, C. Hasse, The influence of intra-droplet heat and mass transfer limitations in evaporation of binary hydrocarbon mixtures, Int. J. Heat Mass Transfer 67 (2013) 1191–1207.
[13] B. Franzelli, A. Vié, M. Boileau, B. Fiorina, N. Darabiha, Large eddy simulation of swirled spray flame using detailed and tabulated chemical descriptions, Flow Turb. Combust. 98 (2017) 633–661.
[14] F. L. S. Filho, A. Hosseinzadeh, A. Sadiki, J. Janicka, On the interaction between turbulence and ethanol spray combustion using a dynamic wrinkling model coupled with tabulated chemistry, Combust. Flame 215 (2020) 203–220.
[15] H. Miyagawa, M. Nagaoka, K. Ohsawa, T. Yamada, Spray vaporization model for multi-component gasoline, JSAE Review 19 (1998) 299–304.
[16] L. F. T. Leite, P. L. C. Lage, Modeling of emulsion droplet vaporization and combustion including microexplosion analysis, Combust. Sci. Tech. 157 (2000) 213–242.
[17] C. Wang, A. M. Dean, H. Zhu, R. J. Kee, The effects of multicomponent fuel droplet evaporation on the kinetics of strained opposed-flow diffusion flames, Combust. Flame 160 (2013) 265–275.
[18] T. Kitano, J. Nishio, R. Kurose, S. Komori, Evaporation and combustion of multicomponent fuel droplets, Fuel 136 (2014) 219–225.
[19] P. B. Govindaraju, M. Ihme, Group contribution method for multicomponent evaporation with application to transportation fuels, Int. J. Heat Mass Transfer 102 (2016) 833–845.
[20] A. Stagni, L. Esclapez, P. Govindaraju, A. Cuoci, T. Faravelli, M. Ihme, The role of preferential evaporation on the ignition of multicomponent fuels in a homogeneous spray/air mixture, Proc. Combust. Inst. 36 (2017) 2483–2491.
[21] P. B. Govindaraju, T. Jaravel, M. Ihme, Coupling of turbulence on the ignition of multicomponent sprays, Proc. Combust. Inst. 37 (2019) 3295–3302.
[22] C. K. Law, T. Y. Xiong, C. Wang, Alcohol droplet vaporization in humid air, Int. J. Heat Mass Transfer 30 (1987) 1435–1443.
[23] A. Millán-Merino, E. Fernández-Tarrazo, M. Sánchez-Sanz, Theoretical and numerical analysis of the evaporation of mono- and multicomponent single fuel droplets, J. Fluid Mech. 910 (2021).
[24] P. Versaevel, Combustion laminaire diphasique etude théorique et expérimentale (1996) 1–244.
[25] G. Castanet, F. Lemoine, Heat transfer within combusting droplets, Proc. Combust. Inst. 31 II (2007) 2141–2148.
[26] A. Vié, B. Franzelli, Y. Gao, T. Lu, H. Wang, M. Ihme, Analysis of segregation and bifurcation in turbulent spray flames: A 3d counterflow configuration, Proc. Combust. Inst. 35 (2015) 1675–1683.
[27] G. Parant, L. Zimmer, A. Renaud, . Richecoeur, Adaptation of a ptv method for droplets evaporating in vicinity of a flame, Exp. Fluids 63 (2022) 100.
[28] J. Wang, P. M. de Oliveira, R. S. Pathania, I. E. Helou, E. Mastorakos, Stability and structure of lean swirling spray flames with various degrees of prevaporization, Int. J. Spray Combust. Dyn. 15 (2023) 91–104.
[29] A. Neophytou, E. Mastorakos, Simulations of laminar flame propagation in droplet mists, Combust. Flame 156 (2009) 1627–1640.
[30] F. L. S. Filho, N. Speelman, J. A. van Oijen, L. P. H. de Goey, A. Sadiki, J. Janicka, Numerical analyses of laminar flames propagating in droplet mists using detailed and tabulated chemistry, Combust. Theory Model. 22 (2018) 998–1032.
[31] F. L. S. Filho, G. C. K. Filho, J. A. van Oijen, A. Sadiki, J. Janicka, A novel strategy to accurately represent the carrier gas properties of droplets evaporating in a combustion environment, Int. J. Heat Mass Transfer 137 (2019) 1141–1153.
[32] B. Rochette, E. Riber, B. Cuenot, Effect of non-zero relative velocity on the flame speed of two-phase laminar flames, Proc. Combust. Inst. 37 (2019) 3393–3400.
[33] F. L. S. Filho, L. E. de Albuquerque Paixão e Freire de Carvalho, J. A. van Oijen, G. C. K. Filho, Effects of reaction mechanisms and differential diffusion in oxy-fuel combustion including liquid water dilution, Fluids 6 (2021) 47.
[34] B. Somers, The simulation of flat flames with detailed and reduced chemical models, Ph. D. Dissertation. (1994)

195.
[35] J. A. van Oijen, L. P. H. de Goey, Modelling of premixed counterflow flames using the flamelet-generated manifold method, Combust. Theory Model. 6 (2002) 463–478.
[36] J. A. van Oijen, A. Donini, R. J. M. Bastiaans, J. H. M. ten Thije Boonkkamp, L. P. H. de Goey, State-of-the-art in premixed combustion modeling using flamelet generated manifolds, Prog. Energy Comb. Sci. 57 (2016) 30–74.
[37] A. Ern, V. Giovangigli, Fast and accurate multicomponent transport property evaluation, J. Comput. Phys. 120 (1995) 105–116.
[38] N. M. Marinov, A detailed chemical kinetic model for high temperature ethanol oxidation, Int. J. Chem. Kinet. 31 (1999) 183–220.
[39] B. Abramzon, W. A. Sirignano, Droplet vaporization model for spray combustion calculations, Int. J. Heat Mass Transfer 32 (1989) 1605–1618.
[40] D. F. Fairbanks, C. R. Wilke, Diffusion coefficients in multicomponent gas mixtures, Ind. Eng. Chem. 42 (1950) 471–475.
[41] E. N. Fuller, K. Ensley, J. C. Giddings, Diffusion of halogenated hydrocarbons in helium. the effect of structure on collision cross sections, J. Phys. Chem. 73 (1969) 3679–3685.
[42] B. E. Poling, J. M. Prausnitz, J. P. O'Connell, The Properties of Gases and Liquids, 5th ed., McGRAW-HILL, 2001.
[43] J. Liang, G. Li, Z. Zhang, Z. Xiong, F. Dong, R. Yang, Experimental and numerical studies on laminar premixed flames of ethanol–water–air mixtures, Energy Fuels 28 (2014) 4754–4761.
[44] ANP, Resolução anp nº 907, de 18 de novembro de 2022 - dou de 23-11-2022, 2022.
[45] S. Hayashi, S. Kumagai, T. Sakai, Propagation velocity and structure of flames in droplet-vapor-air mixtures, Combust. Sci. Tech. 15 (1977) 169–177.
[46] H. Nomura, K. Izawa, Y. Ujiie, J. Sato, Y. Marutani, M. Kono, H. Kawasaki, An experimental study on flame propagation in lean fuel droplet-vapor-air mixtures by using microgravity conditions, Symp. Combust. Proc. 27 (1998) 2667–2674.
[47] F. A. Williams, Combustion Theory, (1985), 2 ed., Addison Wesley, 1985.
[48] K. K. Kuo, Principles of combustion, 2 ed., John Wiley and Sons Inc., 2005.
[49] T. Poinsot, D. Veynante, Theoretical and numerical Combustion, 2 ed., 2005.
[50] J. Kuehne, A. Ketelheun, J. Janicka, Analysis of sub-grid pdf of a progress variable approach using a hybrid les/tpdf method, Proc. Combust. Inst. 33 (2011) 1411–1418.
[51] F. L. S. Filho, L. Dressler, A. Hosseinzadeh, A. Sadiki, G. C. K. Filho, Investigations of evaporative cooling and turbulence flame interaction modeling in ethanol turbulent spray combustion using tabulated chemistry, Fluids 4 (2019) 187.
[52] G. D. Myers, A. H. Lefebvre, Flame propagation in heterogeneous mixtures of fuel drops and air, Combust. Flame 66 (1986) 193–210.
[53] B. Franzelli, A. Vié, M. Ihme, Characterizing spray flame-vortex interaction: A spray spectral diagram for extinction, Combust. Flame 163 (2016) 100–114.
[54] F. L. S. Filho, G. Kuenne, M. Chrigui, A. Sadiki, J. Janicka, A consistent artificially thickened flame approach for spray combustion using les and the fgm chemistry reduction method: Validation in lean partially pre-vaporized flames, Combust. Flame 184 (2017) 68–89.